Characterization of atomic layer deposited thin films by prism coupler

Saeedeh Soleimani

Master's thesis
January 2016
Department of Physics and Mathematics
University of Eastern Finland

Saeedeh Soleimani, 55 pages
University of Eastern Finland
Master degree program in photonics

Supervisors Prof. Markku Kuittinen
Doc. Antti Säynätjoki

Abstract

This thesis presents prism coupler studies to characterize the optical properties of various thin films. In the beginning, the simulation of thin films and their propagation modes have been presented. The fabrication methods and the measurement results of thin films have been discussed. The optical properties of amorphous TiO2, Al2O3, nanolaminates TiO2 and Er2O3-Al2O3 thin films are studied at 532 nm, 633 nm, 1064 nm and 1550 nm wavelengths and a close agreement between results between simulation and experiment is achieved. Finally, propagation loss of < 0.7 dB/mm at 1550 nm wavelength for 183 nm nanolaminate TiO2 is measured.

This thesis presents prism coupler studies to characterize the optical properties of various thin films. In the beginning, the simulation of thin films and their propagation modes have been presented. The fabrication methods and the measurement results of thin films have been discussed. The optical properties of amorphous TiO2, Al2O3, nanolaminates TiO2 and Er2O3-Al2O3 thin films are studied at 532 nm, 633 nm, 1064 nm and 1550 nm wavelengths and a close agreement between results between simulation and experiment is achieved. Finally, propagation loss of < 0.7 dB/mm at 1550 nm wavelength for 183 nm nanolaminate TiO2 is measured.

Preface

During seven months work in micronova at Otaniemi, I have learned to work with prism coupler device and I have gained valuable research experience. I also enjoyed research work environment in micro and nanoscience group. I want to express my gratitude to my professor, supervisor and my family for giving me an opportunity to work on this project.

Otaniemi, Finland, January 2016 *Saeedeh Soleimani*

Contents

Chapter I
Introduction

Through the Max Planck discovery, we understood that all particles have wave nature and all waves have particle nature. The understanding of physics of light has developed gradually in the course of history. Light is an electromagnetic radiation which can be found everywhere in the world. Physics of light is often described the study of optics or photonics and it is used in relevant industry or technology. Optics/phonics applications include lenses, cameras, semiconductors, waveguides, etc. In technology, one way to utilize light is in waveguide technology. [4, 31]

The beam of light will be spread by diffraction with a finite cross-section when the propagation is occurring in the free space. In this case, lenses will be used to focus and confine the beam propagation in a proper location. Structure with higher index core such as optical fibers, dielectric slab and waveguides are used to support confined electromagnetic propagation. The simplest optical waveguide is dielectric waveguide which consists of dielectric layer with refractive index of n_1. Dielectric slab is called core and it is sandwiched between two semi-infinite bounding media (cladding) with refractive index of n_2. To support the guided modes, n_1 should be larger than n_2. There are different kinds of waveguides, one of the common waveguides is slab waveguides. A strip waveguide, a ridge waveguide and a diffused waveguide are two-dimensional waveguides. Strip waveguides are basically slab waveguides with high index material that is surrounded by lower index materials. The guiding layer in strip waveguide is restricted in both transverse directions. The propagation modes for strip waveguides are solved geometry by Maxwell's equations. [36] Strip waveguides are applied in nonlinear applications and in waveguides sensors. [37, 38] In ridge waveguide structure the strip's guiding part is changing to ambient medium with a refractive index is lower than the clad

part. Diffused waveguides are graded-index waveguides whose the refractive indices difference is small between clad and core parts. The refractive index is changing easily as a function of transverse location in diffused waveguide. [22]

Thickness and the refractive index properties of slab waveguides could be measured by prism coupler device. In prism coupling method, a monochromatic laser source is utilized to monitor the propagation modes of slab waveguides to a thin film on a substrate. The prism coupling device measures the incident angle ζ, and based on the Eq. (1), effective index of the mode can be solved using [39, 40]

$$n_{eff} = \cos\varepsilon \sin\zeta + \sin\varepsilon \sqrt{n_p^2 - sin^2\zeta}, \quad (1)$$

where the prism angle is presented by $\mathcal{E}$ and the refractive index of the mode is presented by n_p. The waveguides used in this work are fabricated by ALD technology.

ALD is a thin film deposition technique which was invented independently by researchers in Finland and Soviet Union. In Finland, for the first time ALD was invented for making thin film electroluminescent (TEFL) displays in 1974 by Tuomo Suntola. ALD technique first was named atomic layer epitaxy (ALE) and molecular layering (ML) but later on the name ALD was described the technology more precisely. There are other similar techniques included atomic layer vapor deposition (ALVD) and molecular layer epitaxy (MLE). [32]

ALD has gained recently a lot of interest in many industry and technology applications. In 1990, ALD accepted as a depositing thin dielectric film by semiconductor industry and in 2000, it has been used in photovoltaic and barrier applications. [2] ALD technique is very proper technique for filling slots with different materials, TiO_2 and Al_2O_3 have been verified to be suitable ALD materials. [33, 34, 35]. In this work, we focused on fabrication and characterization of amorphous and nanolaminates TiO_2, amorphous Al_2O_3 and Er_2O_3-Al_2O_3 materials.

In this work, optical geometry, waveguide theory, ALD technique and prism coupling method are discussed in chapter 2. Furthermore, characterizations of atomic layer deposited TiO_2, Al_2O_3, Er_2O_3-Al_2O_3 thin films and nano laminates are discussed. The fabrication and properties of the thin films are discussed. The guided modes in the films are simulated with SiIO (simulation in integrated optics) online tool, which is a mode solver software for dielectric slab waveguides. Electric or magnetic field profile of modes

in films of different refractive index, wavelengths and layer thicknesses are discussed in chapter 3. Moreover, in experimental part, the propagation constant of the propagating modes are determined using a Metricon Prism coupling system. The measurement is done with four wavelengths, i.e., 532 nm, 633 nm, 1064 nm and 1550 nm. The propagation constants found with the prism coupling experiment are used to determine thickness and refractive index of the thin films at different wavelengths. Furthermore, Cauchy dispersion model is plotted for refractive index as a function of wavelength. Finally, loss measurement is done for the decay of propagation light in slabs. All results of experiment is discussed in chapter 4.Finally, the conclusion of this work is given in chapter 5.

Chapter II
Theory

2.1 Waveguide Theory

This chapter gives you a theoretical background of waveguides which is mostly based on the electromagnetic theory.

2.1.1 Geometric Optics and Refractive Index

Geometric optics is applied to study wave propagation in homogenous dielectric materials. In geometry optics, tangential component of electric field vector (*E)* and magnetic field vector (*H)* are continuous across any boundary and Snell's law can be applied

$$n_1 \sin\theta_1 = n_2 \sin\theta_2, \quad (2)$$

where n_1 is refractive index of first medium, n_2 is refractive index of second media, θ_1 and θ_2 are the angles to surface normal. If the incident angle is larger than critical angle and the light is coming from higher refractive index medium then the total internal refraction occurs. Eq. (3) defines the total internal refraction

$$\theta_c = \sin^{-1}\left(\frac{n_2}{n_1}\right), \quad (3)$$

where θ_c is critical angle. Fig.1 shows the dielectric interface of materials having refractive indices, n_1 and n_2.

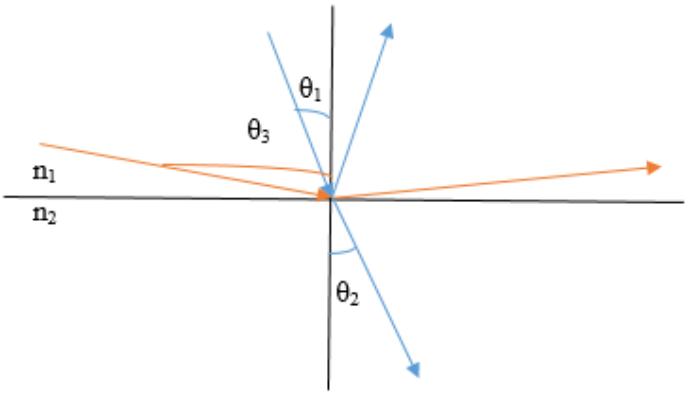

Figure 1. Light refraction at dielectric interfaces when $n_1 > n_2$.

As shown in Fig. 1, angle θ_3 is larger than the critical angle, θ_c, therefore total internal reflection occurs and the part of light is having angle of θ_1 that is smaller than θ_c is reflected and the rest of light is refracted to larger angle, θ_2. Refractive index relates to the relative permittivity, $\mathcal{E}_r$, and permeability, μ_r as it is shown

$$n^2 = \frac{\varepsilon\mu}{\varepsilon_0\mu_0} = \varepsilon_r\,\mu_r\,, \tag{4}$$

where $\mathcal{E}(r)$ is permittivity tensor, $\mu(r)$ is permeability tensor, $\mathcal{E}_0$ is permittivity of vacuum which it is constant and equivalent to 8.854×10^{-12} F/m and μ_0 is permeability of vacuum which it is equivalent to $4\pi \times 10^{-7}$ H/m. For most cases, $\mu_r \approx 1$ therefore $n^2 \approx \mathcal{E}_r$. [22]

In lossy material, refractive index is a complex number and imaginary part is called extinction coefficient *k*. [2]

2.1.2 Maxwell's Equations

Maxwell's equations were formulated by James Clerk Maxwell, a Scottish physicist. Electromagnetic theory defines electromagnetic fields and optical waves with Maxwell's equations. Electromagnetic theory describes that all electric, magnetic, optical and electromagnetic phenomena are ruled by four fundamental laws of electromagnetism. These equations are

$$\nabla \times E + \frac{\partial}{\partial t}(\mu H) = 0, \quad (5)$$

$$\nabla \times H - \frac{\partial}{\partial t}(\varepsilon E) = J, \quad (6)$$

$$\nabla . (\varepsilon E) = \rho, \quad (7)$$

$$\nabla . (\mu H) = 0, \quad (8)$$

where H is magnetic field vector in A/m, B is the magnetic induction vector in Tesla (T) or in Weber .m^{-2}, D is electric displacement vector in C.m^{-2}. The charge density is ρ *(r)* in C/m^3 and scalar in an isotropic medium. The current density vector is J with the unit of A/m^2.

Material equations describe the connection between D and E as well as between H and B. These material equations or so called constitutive equations are presented as [22, 25]

$$D = \varepsilon E = \varepsilon_0 E + P, \quad (9)$$

$$B = \mu H = \mu_0 H + \mu_0 M, \quad (10)$$

where P is electric polarization and M is magnetic polarization. Maxwell's equations should be solved in parts for non-continuous media. The wave equation is divided in dielectric parts and using proper boundary conditions. Boundary condition can be derived from Maxwell's equations using Gauss and Stokes theorems. [21]

2.1.3 Polarization

The electric field of a plane wave includes two orthogonal components and the polarization describes the relationship between the phase of these two orthogonal components and amplitudes. If the components have phase difference of multiple $\pi/2 + m\pi$ where m is an integer and same amplitudes then the polarization defined as circular polarization but if the amplitudes are different then the polarization is elliptical. Linear polarization occurs when the phase difference is a multiple of π.

If the electrical field component of plane wave is perpendicular to the incidence plane which it is covered by wave vector then normal of surface is called transverse electric component (TE). The component that has parallel electrical field to the incidence plane is defined as the transverse magnetic component (TM).

When the optical source free, linear and isotropic medium is considered, $J= 0$, $\rho = 0$ and $\mathcal{E}$ and μ are independent of E and H. Maxwell's equations build electromagnetic equations as below

$$\nabla \times E = -\frac{\partial B}{\partial t}, \tag{11}$$

$$\nabla \times H = \frac{\partial D}{\partial t}, \tag{12}$$

$$\nabla . D = 0, \tag{13}$$

$$\nabla . B = 0. \tag{14}$$

This assumption is reasonable because at high frequency ($v > 10^{13}$ Hz), free charge and current are not source of electromagnetic energy. Bulk permittivity and permeability are applied in Maxwell's equations. The source of optical energy are typically electric or magnetic dipoles which come from atoms and molecules transitions. [22, 26]

From electromagnetic equation can be reached to a general solution of wave equation which is presented here

$$\psi(r,t) = \psi(r)\Phi(t) = \Psi_0 e^{(iK.r)} e^{(i\omega t)} + c.c. \tag{15}$$

where ψ_0 is the amplitude, k is wave vector which its magnitude defines as $k=2\pi\hbar/\lambda$, ω is the angular frequency and is equivalent to $\omega = 2\pi v$ and *c.c.* is complex conjugate. [26]

2.1.4 Optical Waveguides

Light is guided typically in higher index material. Guiding process of electromagnetic wave can be explained by total internal refraction either by wave optical theory. The most

common waveguides are slab, strip and diffused waveguides and optical fiber. The typical waveguide materials are glass and lithium niobate. [22]

In this work, two kinds of waveguides will be explained, step-index and graded-index waveguides. Fig. 2 shows a step-index waveguide, which has a core of uniform material where light propagates as a straight line.

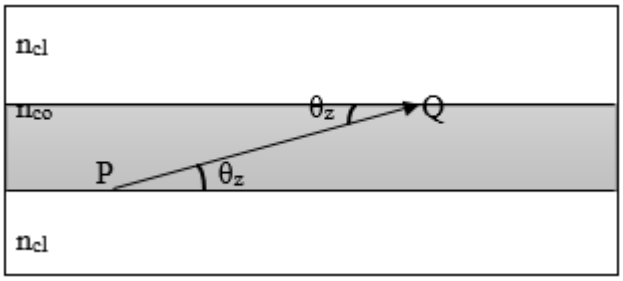

Figure 2. Schematic of step-index planar waveguide when a propagation of light along the straight line between interfaces in the core of waveguide.

Where *P* is originate point, *Q* is a point where light will meet after propagation along the straight line, n_{co} is refractive index inside of the waveguide and n_{cl} is refractive index out of waveguide. Snell's law is used to consider the refraction in the Fig. 2. The angle of refraction is called θ_t in Snell's law equation

$$n_{co}\ \sin(\frac{\pi}{2} - \theta_z) = n_{cl}\ \sin(\frac{\pi}{2} - \theta_t). \tag{16}$$

In equation below critical angle condition is calculated and it occurs when $\theta_z = \theta_c$, and light propagates along the interface

$$\theta_c = \cos^{-1}(\frac{n_{cl}}{n_{co}}) = \sin^{-1}(1 - \frac{n_{cl}^2}{n_{co}^2})^{1/2}. \tag{17}$$

The light will reflect inside the waveguide if $0 \leq \theta_z \leq \theta_c$ and in other words total internal reflection occurs. In total internal reflection, rays propagate inside of waveguide core in zigzag lines and all power of rays will remain in the core medium which is illustrated in Fig. 3. In other hand, when $\theta_c \leq \theta_z \leq \pi/2$, the light partially refract and partially reflect. In this case, rays power is lost in every reflection which is illustrated in Fig.4. In waveguides, there are different kinds of loss occurred such as absorption and scattering loss however the waveguide is facing refracting loss if $\theta_c > \theta_z$. [22, 24]

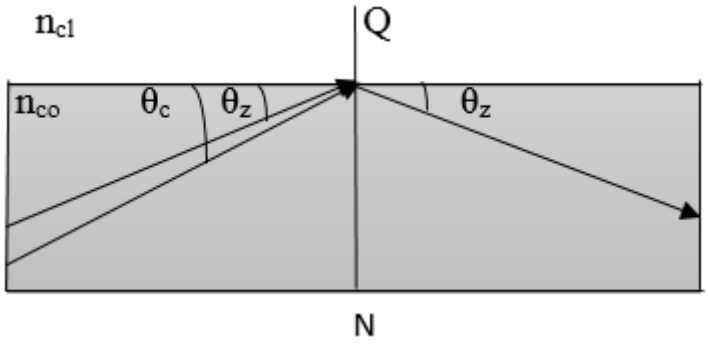

Figure 3. Illustration of total internal refraction at planar interface between unbounded regions of refractive indices n_{co} and n_{cl}.

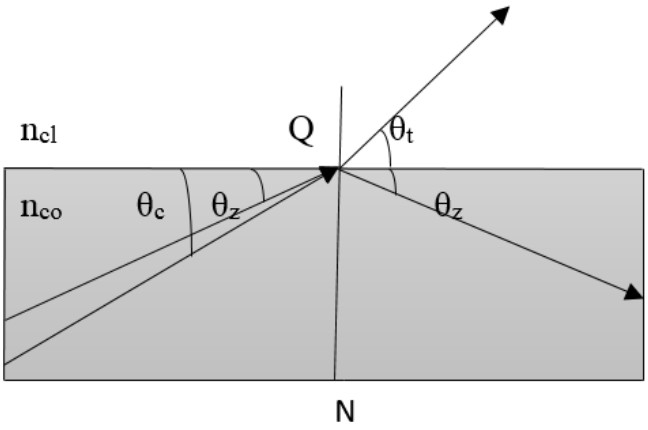

Figure 4. Illustration of partial reflection and refraction. [24]

2.1.5 Planar Waveguide

Planar waveguide schematic shown in Fig. 5 where there are three different refractive indices chosen, $n_f > n_s > n_c$ but the thickness of guiding layers are same as film height. Cartesian coordinate system has chosen to make the problem simple as possible. [27] The reason is that the electric field vectors of three coordinates are not coupled with reflection into their directions. The polarization keeps in the same direction and $x= 0$ is placed to interface between n_c and n_f.

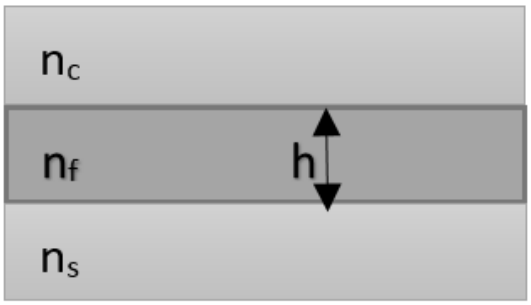

Figure 5. Schematic figure of planar waveguide.

Transverse electric (TE) and transverse magnetic (TM) are two possible field polarizations which are considered here. [28] The TE case has no longitudinal electric field component along the *z* axis. The waveguide axis is in direction of *z*-axis and the *k*-vector is in *x*-*z* plane.

Both TE and TM cases have different boundary conditions that control the fields and therefore their modes characteristics are distinguishable. [26] In TE case, electrical field is polarized along the *y*-direction. The propagation wave has a frequency of ω_0 and a vacuum wave vector of magnitude of $k_0 = \omega_0/c$. The wave equation is divided and solved in each dielectric region which the boundary conditions are applied there. After this, wave equation should be

$$\nabla^2 E_y + k_0^2 n_l^2 E_y = 0, \quad (18)$$

where $n_l = n_f$, n_s or n_c and is depending on the region. The wave is propagating in the *z*-direction and the slab is infinite in *y*- direction therefore the electric field is only function on the *x* and *z* directions, $E_y(x,z)$. The solution for equation above would be

$$E_y(x,z) = E_y(x) e^{-i\beta_l z}, \quad (19)$$

where β is propagating coefficient in the *z*- direction. When the Eq. (19) is substituting in Eq. (18) and $d^2E_y/dy^2 = 0$, the result will be

$$\frac{\partial^2 E_y}{\partial x^2} + (k_0^2 n_l^2 - \beta^2) E_y = 0. \quad (20)$$

For $x > 0$, $n_l = n_c$, for $0 > x > -h$, $n_l = n_f$ and for $x < -h$, $n_l = n_s$. Solution of equation above is dependent on the β with respect to $k_0 n_l$, and magnitude of β is unknown yet. β is defined as $k_0 n_c < \beta < k_0 n_f$ where n_f is refractive index of film and n_c is refractive index of cladding. The wave equation will be solved in two parts which are if $\beta > k_0 n_l$ and $\beta < k_0 n_l$ and the solution is presented here

$$E_y(x) = E_0 e^{\pm\sqrt{\beta^2 - k_0^2 n_l^2}\, x} \quad for\ \beta > k_0 n_l, \quad (21)$$

$$E_y(x) = E_0 e^{\pm i\sqrt{k_0^2 n_l^2 - \beta^2}\, x} for\ \beta < k_0 n_l, \quad (22)$$

where E_0 is the unknown field amplitude. If the $\beta > k_0 n_l$ then $\gamma = (\beta^2 - k_0^2 n_l^2)^{1/2} > 0$ and the solution will be in real exponential form. In this case the electric field will be $E_y(x) = E_0 e^{\pm\gamma x}$ and electric field can be formed to hyperbolic function

$$E_y(x) = E_0 (\cosh \gamma x \pm \sinh \gamma x), \quad (23)$$

when $\beta < k_0 n_l$ then the solution will be in oscillatory form, $E_y(x) = E_0 e^{\pm i\kappa x}$. In both cases, the solution can be expanded in trigonometric format

$$E_y(x) = E_0 (\cos kx \pm i \sin kx). \quad (24)$$

In Eqs. (21 & 22) β and κ_0 are longitudinal and transverse wave vectors in the guiding layer and geometrically are related to the total wave vector, $k = k_0 n_f$. [26] This relation is drawn in Fig.6.

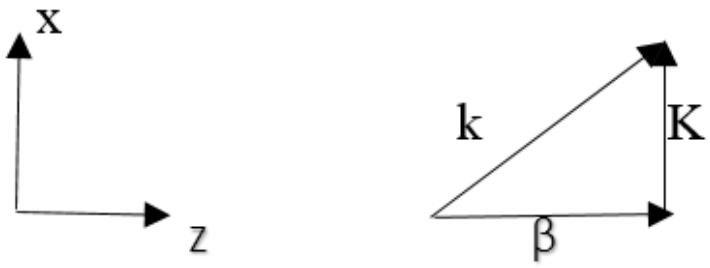

Figure 6. Total wave vector.

The final solution for the electric field is using the boundary conditions when the guided modes are oscillatory located inside the core or are exponentially damping out of the core.

2.2 ALD Process

The invention of ALD helps to growth higher quality thin films by making better the phosphor and dielectric film stacks in thin film electroluminescent (TFEL) displays. [1,2] In the beginning, there was a technique was called atomic layer epitaxy (ALE) which was introduced for the preparation of dielectric multilayer for optical applications. ALE possesses some features such as simple and accurate thickness control and uniformity over large area of substrate which makes ALE an attractive technique for depositing optical thin films. The name ALD was introduced later by Riihelä in 1996. [30]

ALD technique is used very often to fabricate thin films in semiconductor industry because of some advantages. ALD technique produces film with superior conformity even on high- aspect- ratio structure, high quality film with exact thickness, superior conformity and it enables to fabricate monolayer thin film. [3, 4]

ALD operation is based on the vapor and gas chemical process. [5] The vapor source is connected to the reactor alternately and is based on the self-limiting growth mechanism of film. The first operation of ALD is started with pulsing the first reactant to the chamber under vacuum to react to the substrate surface for an estimated time. The deposition temperature varies between 100°C-300°C but it can be high as 500°C for some reactors. The reactants that are pulsed to the chamber are defined as a precursor. Usually the first precursor is a chemical which contains metal or semiconductor elements. After exposure of first reactant, the purging process begins to remove the chemicals remained from substrate surface materials which did not react in first reaction. In the purging process, inert gas like N_2 or Ar is used. Then, the second reactant is pulsed to the chamber for designated amount of time to react with the substrate which has already one sublayer of chemical. The second precursor is usually a water or ozone. Any material in ALD technique needs precursor chemicals to grow, for example, the TiO_2 growth needs Ti and O_2 to make the final product.

The results of both reactions is fraction of one monolayer film. After reaction is ended, the purging begins to remove remained chemicals. The deposition continues to repeat this cycling process till the desired amount of film thickness is achieved. [6]

One cycle of deposition is a total of pulsing and purging times of both reactors. If the pulsing time is defined as t_{pu1} for first reactor, t_{pu2} is for second reactor, t_{pr1} is purging

time for first reactor and t_{pr2} is purging time for second reactor. The total time of cycle is given by

$$Duration\ of\ one\ cycle = t_{pr1} + t_{pu1} + t_{pr2} + t_{pu2}, \quad (25)$$

and the total process time is given by

$$\text{Deposition time= Duration of one cycle} \times \text{number of cycles.} \quad (26)$$

One cycle of ALD typically produces 1Å of film. ALD cycling depends on the precursor and deposition parameters like deposition rate which is expressed often as a (Å/cycle). The deposition rate can vary from 0.10 Å/cycle with heavy /poorly reacting materials or can vary to 2 Å/cycle with light/strongly reacting materials. Growth rate is also expressed often as a (Å/min) and it is a deposition parameter which is important in deposition process and depends on pulsing time, purging time and flow rate of both reactants. All deposition factors should be optimized for each material. After optimization, the growth rate will remain same for all process cycles occurring inside reaction chamber. Deposition rate will be remain same in a specific range of temperature which is expressed as ALD-window of material. The growth rate of material needs to be chosen for deposition temperature inside of ALD-window process in order to achieve the desired properties of ALD. [4, 7]

The growth of the material in ALD chamber depends on the reactivity of chemicals on the substrate. Chemical reaction cannot occur under normal condition because the chemicals need high amount of energy to complete the reaction. There are some operation modes of ALD have been developed to support this chemical reactions process in the deposition chamber. One of these operation mode of ALD is thermally-driven in ALD which provides high temperate for the chemical reactions to occur.[7] In some chemical reactions like metal nitrides and metal oxides, the thermal ALD does not provide sufficient energy for chemical reaction and these material need higher amount of energy to complete the reaction. There is an alternative deposition technique invented to fabricate the weakly reacting chemicals which is called plasma ALD or plasma enhanced ALD (PEALD). [8] Plasma is named as a fourth state of the matter and it occurs when the phase gas material is heated in specific temperature to ionize its molecules and atoms to produce a cloud of charged particles. Plasma is regarded as a neutral electrically by average

because it contains equal number of positive and negative ions. These particles have high amount energy to assist the chemical reaction to occur in the ALD chamber. The plasma gases have used typically in PEALD are produced by N_2, O_2 and H_2. [9]

Although ALD materials are used in different optical applications; such as optical, but in recent years, it has been focused more on electrical properties rather than optical properties of ALD materials fibers and different kind of optical nanostructures. The reason is that it is difficult to find optical parameters of ALD materials and proper process for different optical or photonics applications. ALD optical film properties varies for amorphous and crystalline films. The optical properties of crystalline film depends on crystal structure. Amorphous and crystalline TiO_2 have different optical properties and they are depended on the growth temperature. [1] Amorphous TiO_2 is made of tetrachloride ($TiCl_4$) + water at low temperature. [10] In ALD process, $TiCl_4$ and H_2O are used as a precursor. The chemical reaction in ALD reactor is given by [3]

$$TiCl_4 + 2H_2O \xrightarrow{yields} TiO_2 + 4HCl. \quad (27)$$

The refractive index of amorphous TiO_2 is predicted around 2.2 to 2.65 at wavelength of 633 nm. [1] Crystalline TiO_2 tends to have high scattering loss if the grain size is more than few nanometers. The scattering loss is decreasing by adding intermediate Al_2O_3 layers to crystalline TiO_2. Intermediate Al_2O_3 layers make the film optically amorphous and gives the film specular transmitting condition. [11]

During the ALD process, some materials are grown at interfaces. These materials bring some unwanted properties to the interfaces which makes the film is absorbing. The amount of absorption increases linearly with number of interfaces. It is difficult to find proper materials for nanolaminate films and it makes fabrication of nanolaminates is demanding. [2, 10]

2.2.1 Advantages and Disadvantages

There are some conventional optical coatings that are available for thin film fabrication but ALD coating bring some specific properties for thin films. It enables to fabricate multilayers and nano laminates film with exact thickness because in layer by layer deposition it is possible to design the composition of grown ALD films. [2, 12]

Furthermore, the growth of material is possible on non-flat surface sample that is placed in the reactor and material growth is not limited only on flat surface. Therefore, deposition complicated structure thin films are also possible without using additional lithography steps in order to fabricate desired structure. [2, 13] ALD is a promising technique for making and tuning photonics waveguides. The tunability of waveguide can be achieved by mixing different layers of materials. ALD has also been used to fabricate an active erbium doped Al_2O_3 waveguide. [14]

There are some disadvantages found in ALD technique. Firstly, the layer-layer deposition of the materials and purge steps between each precursor pulsing makes the deposition rate slow. Secondly, the number of available precursors are limited for chemical reaction because of ALD materials need effective methods for chemical reaction. In addition, the self-limiting growth is not occurring between some single element metals like copper. Therefore there is limited possibility to grow some desired materials. [7, 9]

Although ALD is unique and new coating technique, physical vapor deposition (PVD) technology is very complete and less expensive compared to ALD. ALD deposits one atomic layer at a time however chemical vapor deposition technique (CVD) deposits multiple and it is possible to control the PVD growth. ALD technique has low growth rate but it can be compensated to some extent with large batches and optimized flows. [1,7]

ALD is one the few techniques that can fabricate films where the structure can be controlled in nanoscale. ALD is perfect in depositing on top of waveguides because the film grows uniformly on the most complicated structures. With other techniques, you would need to do lithography to define the correct structures. Typical growth rates are available in CVD technique but in ALD technique, film thickness can be estimated accurately if the growth per one cycle is available. Finally, ALD is deposited one cycle at a time, therefore the surface area has same thickness as long as the process is optimized. [1]

In this thesis, the optical properties of amorphous TiO_2, nanolaminates TiO_2, amorphous Al_2O_3 Erbium doped Al_2O_3 will be investigated. [2] Erbium doped Al_2O_3 film is consisted of three layers of Al_2O_3 film and one layer of Er_2O_3 film. The fabrication process was included 2000 cycles and it was repeated to produce 900 nm film thickness.

2.2.2 ALD Machine

ALD machine is used to fabricate the thin films are studied in this thesis is Picosun R-200 tool and is operation with Plasma enhanced mode. Thin film is deposited in deposition chamber (reaction chamber) and it is included inner and outer chambers. Outer chamber is vacuum chamber which separates the room air from the chamber. Inner chamber is reactor chamber which keeps the substrate and chemical reaction is occurring inside the inner chamber. Precursor gas lines is located inside inner chamber, it distributes precursors and leads them towards the reaction chamber. There is no chemical reaction occurring in lines because of the precursor lines are splitting up from each other. The precursors spreads completely on the substrate which make the deposition layers uniform. The deposition chamber is included of six precursor lines and four additional lines for plasma-enhanced modes. The plasma gases are used in deposition process are typically are NH_3, N_2, H_2, Ar_2 and O_2. The highest plasma power can be used is 2500 W. ALD parameters are changing for each fabrication turn during ALD process optimization. ALD parameters are included, source temperature of Erbium precursor, deposition temperature, power of plasma, flow rate of Erbium precursor and pulse duration of Erbium precursor and Oxygen plasma. ALD machine is used to optimize thin films by changing the ALD process parameters for each fabrication turn. [1, 15]

The next part is about ALD application in industry.

2.2.3 Industrial Aspects

There are some critical facts in ALD thin films mass manufacturing should be taken in account. Although optical and electrical properties are important to characterize thin film quality but cost of precursors, process speed, stability of coating and using safe materials are more important aspects in thin film It is important use less materials in a maximum speed in order to optimize process . Ideal chemical and physical materials are safe, easy to handle, inexpensive and have a high vapor pressure in room temperature. In industrial application, chemical process should be optimized for short length pulse, fully saturated, fast and good enough yield. However in research process the length of pulse is long enough to reach the fully saturated materials. There is often used one of the precursors as a non-volatile in chemical process. Di-water precursor is an inexpensive, safe and can used with all metal oxide process. Another precursor is used as a volatile precursor which is more difficult to handle and more expensive. $TiCl_4$ is a volatile precursor which is used

in industrial use. Although they are risky but it is possible to maintain them in low cost and safe. [2]

2.3 Prism Coupler

Experiment setup is used in this measurement is a Metricon Prism coupling device which includes a rotatory table and optics module. Metricon model 2010/M prism coupler device uses optical wave guiding technique to measure precisely the refractive index/birefringence and thickness of dielectric and polymer films as well as refractive index of bulk materials. [29] A Metricon Prism Coupler is used to determine the propagation modes inside the films grown on a glass substrate. Measurement principle for thin film is drawn in Fig.7.

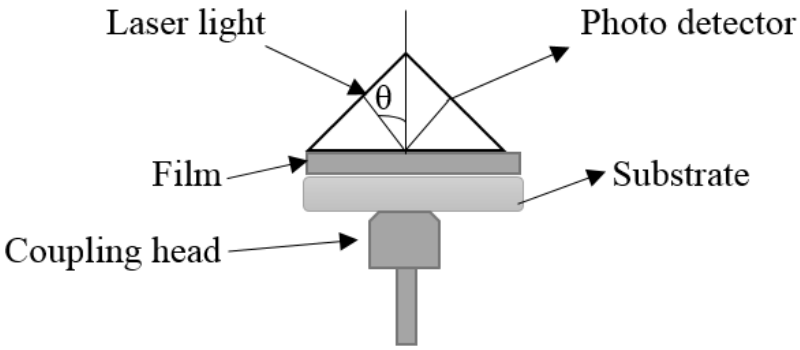

Figure 7. Measurement principle for thin film.

The sample is brought into contact with the base of the prism by a coupling head. There is only small air gap between sample and prism. A laser light strikes the base of prism and the light is completely reflected at the base of prism into the photodetector. At certain values of incident angle (mode angles), photons can tunnel across the air gap into the film and enter into the guided optical propagation mode. This process causes a drop in intensity of light reaching the detector. [29]

The measurement is done with four lasers, 532 nm, 633 nm, 1064 nm and 1550 nm. Two prisms are using during measurement, low index prism (code: 65332.9, index range: 1.20-2.02) and higher index prism (code: 6029.1, index range: 2.00-2.65).

Prism coupler measures the intensity as a function of angle which is converted to propagation constant, β. The propagation modes are displayed as dips in the intensity curve. Prism coupling curves show well-defined sharp dip suggests relatively low loss. The angular location of first mode (dip) indicates the film index and angular difference between the modes determines the thickness of the film. [29] It is also possible to measure both TE and TM modes for each film. Metricon software calculates the refractive index and thickness of the film based on the given effective indices found in propagation modes. Thickness and index of film are calculated when two of the mode angles are detected. Each peak corresponds to a particular effective index and gives an equation which makes a link between the thickness and the refractive index. The equations have two unknown values (refractive index and thickness) and two equations are needed to estimate the two unknown values.

With effective indices of modes, it is possible to calculate the refractive index and thickness for each film.

Thickness measurement is dependent to the optical constant and the film thickness measurement affects the optical length of light traveling through the film. Index of the film determines the light waves 'velocity and refracted angle'. Both velocity and refracted angle contributes the delay of between surface reflection and light traveling through the film. Refractive index and wave vector must be known in order to achieve the correct result from an optical measurement.

The optical constant varies for different wavelengths and it is determined by ellipsometer at all wavelengths. The material's response at each wavelength can be predicted by table of optical constant however it is not easy to adjust unknown optical constants on a wavelength by wavelength basis. To solve this problem, a dispersion model is introduced for optical constant as a function of wavelength. The dispersion model is adjusted by optical parameters which allow the optical constant form to match the experimental results. Cauchy dispersion model is often used to describe index of transparent material. The Cauchy relationship is generally described as:

$$n(\lambda) = A + \frac{B}{\lambda^2} + \frac{C}{\lambda^4}, \quad (28)$$

where *A*,*B* and *C* are adjusted parameters to match the refractive index of material and λ is wavelength of material. [41]

The total measurement process is completely automated and requires about twenty seconds. The measurement starts with inserting the film in contact with the prism and the laser measurement starts automatically according to the Metricon software.

Metricon model 2010/m prism coupler possesses some features such as: It enables to measure refractive index of bulk materials, substrate and it is possible to measure index vs temperature (*dn/dt*) and waveguide loss.

Chapter III
Sample Design

3.1 Simulation in Integrated Optics

In this part, simulation of eight films at particular wavelengths is presented. Simulation is completed with SiIO (simulation in integrated optics) software. SiIO is a basic tool for integrated optics design. It is a mode solver software for dielectric multilayer slab waveguides with one dimension in cross section. It is defined the waveguide concept in terms of refractive index, vacuum wavelengths and layer thicknesses. The N-layers slab waveguide structure is illustrated in Fig.8. The structure includes refractive index of substrate n_s, refractive indices of inner layers $n_{1,\ldots,}n_N$, refractive index of cover n_c and the thickness of inner layers $t_{1,\ldots,}t_N$. [16] Light propagates in the direction of *z*-axis, *x*-axis is perpendicular of the film plane and all fields are assumed constant along the *y*-axis.

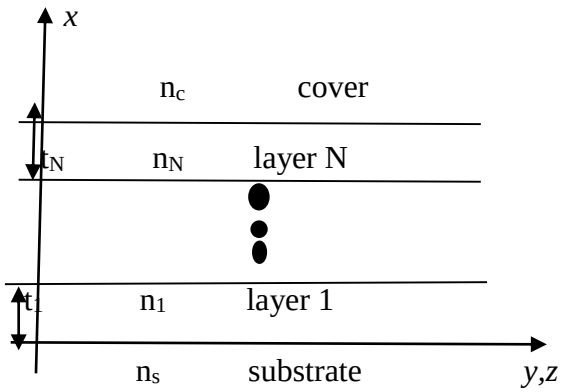

Figure 8. Geometry of N-layers slab waveguides structure. [16]

SiIO calculated the propagation constants (β) and effective indices of guided modes and the optical field patterns of electric and magnetic fields are investigated. Beta (β) is propagation constant (in μm^{-1}) and effective index is $n_{eff} = \beta/k$, where $k_0 = 2\pi/\lambda$ is the vacuum wavenumber which is relates to the specific vacuum wavelength, λ. The mode identifier indicates the number of nodes in the basic electric component E_y of TE modes and in the basic magnetic component H_y of TM modes. [16]

Mode profile presents the field or square field (intensity) of the principal electric component E_y for TE modes, and of the principal magnetic component H_y for TM modes. Background shading indicates the dielectric structure. Darker color corresponds to the higher refractive index. TE mode profiles are normalized with the respect to the integral over E_y^2 in the direction of *x*-axis. TM mode profiles are normalized with the respect to the integral which is included H_y^2 divided by the local permittivity. [16]

To determine suitable layer thickness and estimate effective index of the waveguide modes in the films, refractive index of the film, thickness of the film and substrate index should be given and the software structure finds guided modes and estimates the effective indices. [16]

3.2 Simulations and Results

Four different kinds of films are studied in this work: amorphous TiO_2, nanocrystalline TiO_2 (five films with different thicknesses), Al_2O_3 and Er_2O_3-Al_2O_3. In the beginning, the number of modes and their effective indices are calculated by SiIO software for four wavelengths, 532 nm, 633 nm, 1064 nm and 1550 nm. Later, the four types of films are measured by prism coupling with same four wavelengths. Finally, the measurement results are compared with simulation results.

3.2.1 Amorphous TiO_2

TiO_2 film with thickness of 500 nm has simulated for two wavelengths 633 nm and 1550 nm. The refractive index of substrate is known for those two wavelengths. [18] The simulation in SiIO is one layer with refractive index of n=2.30, it is assumed for amorphous TiO_2 at 633 nm wavelength. [17] The glass substrate is corning 0211 material

with refractive index of n=1.523 for 633 nm wavelength and n=1.509 for 1550 nm wavelength [18]. Three TE/ TM modes are found at 633 nm wavelength and one TE/TM mode is found at 1550 nm wavelength respectively. The results of simulation are given in Table 1 with the information about refractive index, n, effective index and thickness. Fig. 9 shows electric field profile in a 500 nm of TiO_2 film thick at 633 nm wavelength.

Table 1. Simulation result for guided modes in an amorphous TiO_2 film with a thickness of 500 nm.

λ (nm)	neff/ TE0	neff/ TE1	neff/ TE2	neff/ TM0	neff/ TM1	neff/ TM2
633	2.24	2.05	1.73	2.22	1.98	1.60
1550	2.07	-	-	1.92	-	-

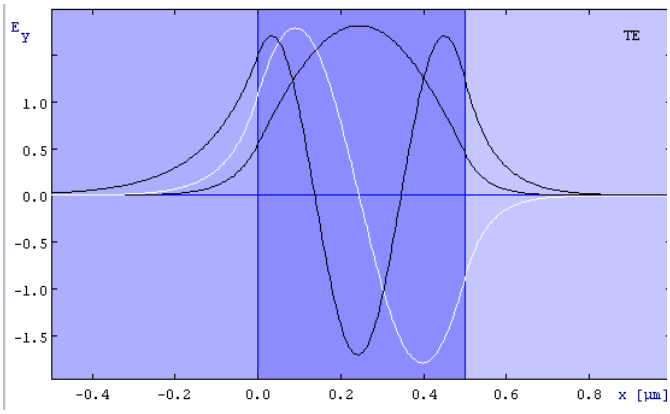

Figure 9. Electric field profile of the TE modes in 500 nm amorphous TiO_2 film at wavelength of 633 nm.

3.2.2 Nano Crystalline TiO_2

Nano crystalline TiO_2 film is a result of a process using titanium chloride ($TiCl_4$) + water (H_2O). In the TiO_2 process, we use a TMA + ozone (O_3) process to make intermediate Al_2O_3 layer to control the crystallinity of TiO_2. Five films were grown with Beneq TFS

500 reactor at 250^0 C. The pulse times were 200 ms for all liquid precursors and 500 ms for the ozone pulses. The purge times were 1.3 s after liquid precursors and 1.5 s with ozone. Corning 0211 glass slides and (100) silicon pieces with thin native oxides are used as substrate. Eleven cycles of TMA + ozone is used to control the crystallinity of TiO_2 and roughness of samples. The growth rate for TMA + ozone process at 250^0C varies between 0.09 to 0.11 nm/cycle. The growth rate depends on the ozone concentration and other parameters. The ozone pulse helps to prevent the formation of the interfacial absorbing compounds and makes the films with high transparency. [17]

Thickness and refractive indices, *n* of five samples have been measured by Perkin Elmer spectrophotometer and the results is presented in Table 2. [17]

Table 2. Deposited samples for nano crystalline TiO_2.

ID	Recipe	Thickness (nm)	*n* at 633 nm
S0	$4000\times(TiCl_4+H_2O)$	203±10	2.30±0.23
S1	$40\times[11\times(TMA+O_3)+100\times(TiCl_4+H_2O)]$	195±2	2.31±0.02
S2	$20\times[11\times(TMA+O_3)+200\times(TiCl_4+H_2O)]$	183±2	2.36±0.02
S3	$15\times[11\times(TMA+O_3)+267\times(TiCl_4+H_2O)]$	173±2	2.44±0.02
S4	$10\times[11\times(TMA+O_3)+400\times(TiCl_4+H_2O)]$	168±2	2.44±0.02

The total number of cycles of process varies between films in order to achieve the desired thickness. [17] Sample ID S0 has only precursors for TiO_2 (i.e., there is no TMA+ozone as precursors) which considers as a crystalline TiO_2. The simulation is divided into different layers (The SiIO in this study is limited to seven layers). According to the total thickness of the film and the number of layers, the relevant thickness for each layer can be calculated. For example, Sample S1 has a total of 195 nm thickness and 40 cycles for total process. There are eleven cycles for Al_2O_3 is assigned with thickness about 1 nm. Therefore, 11 cycles × 0.1 = 1.1 nm is the thickness for each Al_2O_3 layer precisely and the thickness for TiO_2 is calculated as

$$1.1\,nm \times 40\ cycles\ per\ total = 44\,nm\ (total\ thickness\ of\ Al_2O_3)$$

$$195\ nm\ as\ a\ total\ thickness - 44\,nm = 151\,nm\ (Total\ thicness\ of\ TiO_2) \quad (29)$$

$$151\,nm\ \div 100\ cycles\ for\ TiO2 = 1.51\ (Thickness\ for\ each\ layer)$$

The same calculation is done for other samples. The only difference is number of total cycles and number of cycles for TiO_2 film. Sample S0 only contains TiO_2 film with 203 nm thickness and 4000 cycles. The thickness for each cycles is calculated as 203 nm ÷ 4000= 0.050 nm.

The simulation is done based on the six layers (three layers are assigned to Al_2O_3 film and three layers are assigned to TiO_2 film). There are three layers are assigned to TiO_2 and three layers are assigned to Al_2O_3. Simulation result is given for two wavelengths 633 nm and 1550 nm in Table 3. Refractive index of substrate *n*=1.523 for 633 nm wavelength and *n*=1.509 for 1550 nm wavelength.

Fig.10 shows electric field profiles in a 173 nm thick nano crystalline TiO_2 film (S3) at 633 nm wavelength.

Table 3. Simulation result for nano crystalline TiO_2.

Film ID	n_{eff}/TE0 (633 nm)	n_{eff}/TM0 (633 nm)	n_{eff}/TE0 (1550nm)	n_{eff}/TM0 (1550nm)
S0	2.04	1.88	1.71	1.51
S1	2.04	1.86	1.69	1.51
S2	2.06	1.86	1.70	-
S3	2.12	1.88	1.73	-
S4	2.11	1.85	1.71	-

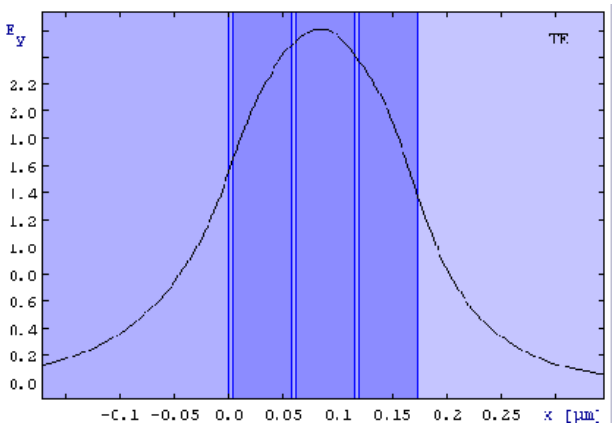

Figure 10. Electric field profile of the TE modes in 173 nm Nano crystalline TiO_2 film at wavelength of 633 nm.

The result in Table 2 shows that when the number of total cycles are increasing, TiO_2 cycles are increasing with the same amount of Al_2O_3 material. It causes the thickness of Nano laminates is much less than bulk TiO_2 (S0) and the refractive index is becoming larger. Simulation result (Table 3) shows that the effective index of fundamental mode is increasing through samples S0-S4. However the effective index in sample S4 is less than sample S3 in both TE and TM modes. The effective indices with 1550 nm wavelength are changing more than with 633 nm wavelength.

In order to characterize the crystal structure of the crystallites in TiO_2 layers, powder x-ray diffraction using Cu K-α radiation was carried out for the samples. The result of XRD shows that the grown TiO_2 is anatase for samples S0, S3 and S4. The reason is that in the diffraction curve of TiO_2 there are three peaks are located at three angles (25.3^0, 48.0^0 and 55.1^0) which correspond to the anatase TiO_2. The width of the diffraction peak is related to the crystal size of sample. Samples S3 and S4 have smaller diffraction peak compared to sample S0 as the diffraction peak is getting wider. Also, the powder XRD shows that the crystal structures of samples S1 and S2 contain only small amount of crystallites. [18] More information about crystallite structure has obtained from scanning electron microscope (SEM). Images of SEM show that the sample S0 has a polycrystalline structure, samples S1 and S2 have only small nanometer scale bumps, sample S3 has unusual and wavy structure with thin and wide crystals and sample S4 has have some large lateral crystal size. [18]

3.2.3 Al_2O_3

The next study film is Al_2O_3 with one layer film on soda lime glass substrate. There have been done several simulations for Al_2O_3 from 0.4 µm-1 µm thickness. Film with 900 nm thick was chosen to be as target sample however the film thickness is reached to 970 nm after film growth. In this film thickness, the simulation result gives the higher number of TE and TM modes. Refractive index was found around n= 1.62 for 30 nm ALD-Al_2O_3 film on Si substrate (0.5 mm, 2 diameter) measured at around 30^0C temperature at 640 nm by spectroscopic ellipsometer. [19] Refractive index measurement depends on the temperature, thickness and other physical condition however the exact refractive index will be measured in chapter 4 (experiment) and compared to simulation result. Refractive index of substrate was found about n=1.46 for 532 nm and 633 nm wavelengths and n=1.45 for 1064 nm and 1550 nm wavelengths. [20] The substrate refractive index measurement will be presented in the experiment part. Simulation result found three TE/TM modes at 532 nm and 633 nm wavelengths, and also it was found a TE/TM at 1064 nm and 1550 nm wavelengths. The results of simulation is presented in Table 4. Fig. 11 shows magnetic field profiles in 970 nm thick Al_2O_3 film at 633 nm wavelength.

Table 4. Simulation result for Al_2O_3 thickness.

λ (nm)	n_{eff} / TE0	n_{eff} / TE1	n_{eff}/ TE2	n_{eff} / TM0	n_{eff}/ TM1	n_{eff}/ TM2
532	1.60	1.55	1.48	1.60	1.55	1.47
633	1.60	1.53	-	1.60	1.52	-
1064	1.57	1.45	-	1.56	-	-
1550	1.54	-	-	1.52	-	-

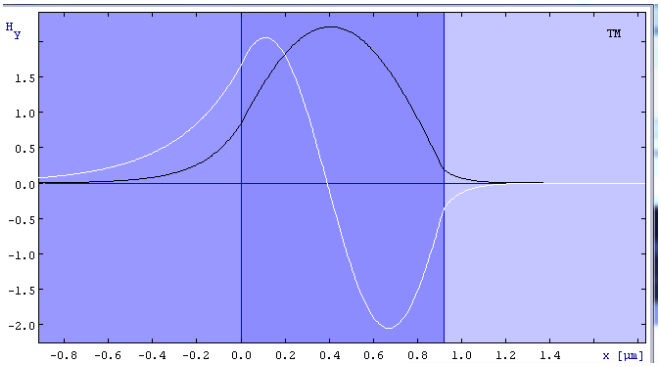

Figure 11. Magnetic field profile of the TM modes in 970 nm Al_2O_3 film at wavelength of 633 nm.

Chapter IV
Experiment

4.1 Thickness-Index Measurement

The measurement results for four different kind of films are presented in chapter 4.

4.1.1 Amorphous TiO_2

The measurement is done with 532 nm, 633 nm, 1064 nm and 1550 nm lasers for both TE and TM polarizations.

The intensity curve is plotted as a function of β in Fig. 12. There are two TE modes shown in Fig. 12 with n_{eff}=2.40 and n_{eff}=2.26 and these are resulted from higher index prism measurement. One TE mode with n_{eff}= 1.66 is obtained by low index prism measurement. Fig. 12 shows also a plot of both prisms measurements (green curve for high index prism and orange curve for low index prism are shown respectively) for TE modes.

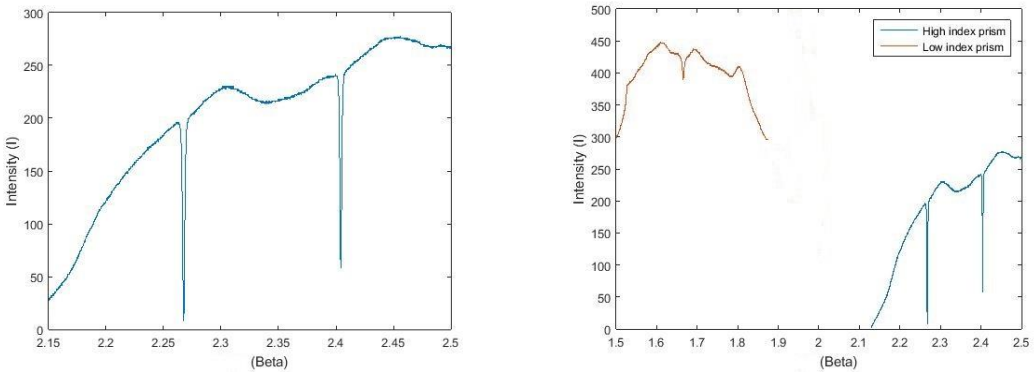

Figure 12. Left: Prism coupling intensity curve in 500 nm amorphous TiO_2 at 532 nm wavelength (higher index prism measurement). Right: Prism coupling modes in 500 nm amorphous TiO_2 film at 532 nm wavelength.

Fig. 13 shows the result of 500 nm amorphous TiO_2 film measurement with 1064 nm laser for TM polarization. One mode is found with higher index prism measurement with n_{eff}= 2.09, corresponding to n=2.29.

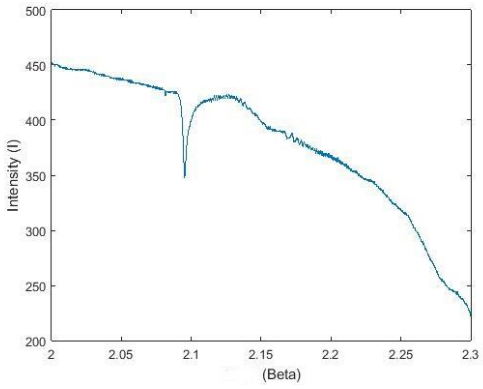

Figure 13. Prism coupling intensity curve in 500 nm amorphous TiO2 film at 1064 nm wavelength.

The result comparison of effective indices gives maximum 0.25 difference between measurement and simulation results for 633 nm wavelength and 0.04 difference for 1550

nm wavelength. The reason could be that the thickness and refractive indices in the film are not precisely same as assumed in simulation. Experiment result is more reliable because the actual sample properties have been measured and all drawbacks of film have been considered in index-film measurement. The ideal properties of film are considered in simulation part and there are a few differences between simulation and experiment results. There is also scattering occurring during measurement which will be affected the propagation modes. The result of experiment is given in Table 5.

Table 5. Experimental result for amorphous TiO_2 film.

λ (nm)	n_{eff} TE0	n_{eff} TE1	n_{eff} TE2	n(TE)	Thick µm	n_{eff} TM0	n_{eff} TM1	n_{eff} TM2	n(TM)	Thick µm
532	2.40	2.26	1.66	2.46	0.41	2.14	2.00	1.66	2.19	0.53
633	2.32	1.80	1.65	2.43	0.34	2.08	1.81	1.65	2.15	0.55
1064	2.16	1.73	-	2.30	0.49	2.09	1.56	-	2.29	0.50
1550	2.04	-	-	2.27	-	1.88	-	-	2.26	-

Table 5 shows that the refractive indices of TE and TM modes have more similar results in measurement with 1064 nm and 1550 nm wavelengths than with 633 nm and 532 nm wavelengths. The refractive index must same for both polarization and the thickness should be found same for all measurements. Prism coupler has calculated thickness in different values at different wavelengths. The reason could be that the all modes have not detected during measurement with 532 nm and 633 nm wavelengths. There is a gap mode between two prisms measurements and therefore one mode is missing during measurement at 532 nm and 633 nm wavelengths. A new simulation is done to find the accurate refractive index for 532 nm and 633 nm wavelength with 500 nm film thick for both polarizations. The result of simulation is presented in Table 6.

Table 6. Simulation result for 500 nm amorphous TiO_2 film.

λ (nm)	n_{eff} TE0	n_{eff} TE1	n_{eff} TE2	n_{eff} TE3	n(TE)	n_{eff} TM0	n_{eff} TM1	n_{eff} TM2	n_{eff} TM3	n(TM)
532	2.40	2.26	2.03	1.68	2.44	2.39	2.22	1.93	1.55	2.44
633	2.32	2.14	1.81	-	2.38	2.30	2.07	1.67	-	2.38
1064	2.16	1.74	-	-	2.30	2.10	1.57	-	-	2.29
1550	2.04	-	-	-	2.27	1.89	-	-	-	2.26

Tables 6 shows that simulation is found the missing mode for 532 nm wavelength for both polarizations. Therefore the correct refractive index and thickness are calculated for 532 nm and 633 nm wavelengths.

4.1.2 Sample Uniformity

In order to examine sample uniformity, different spots of amorphous TiO_2 are measured with 532 nm, 633 nm, and 1550 nm lasers. Three spots are considered in top, left and center of the film as in illustrated in Fig.14. Refractive index, effective index and thickness of these three spots positions have been presented in Table 7.

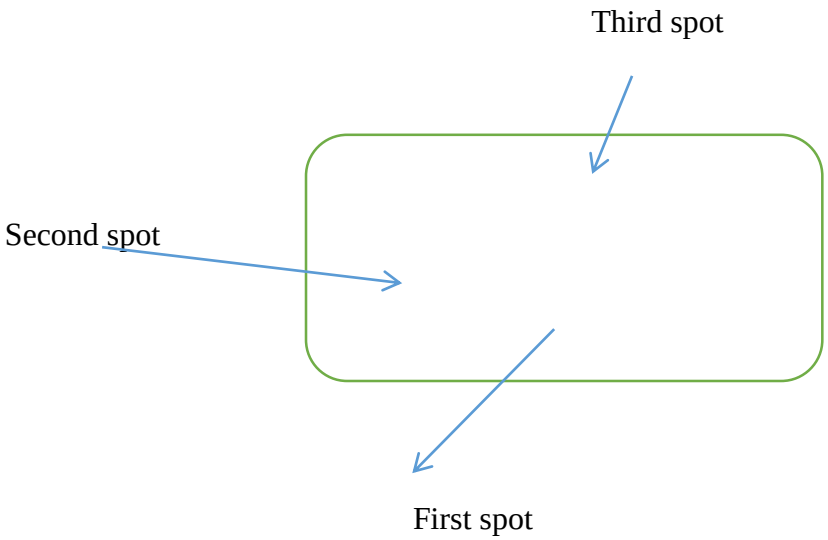

Figure 14. Illustration of different spots locations in amorphous TiO_2.

Table 7. Experimental results for three different spot location of amorphous TiO_2.

λ(nm) spot location	n_{eff} TE0	n_{eff} TE1	n_{eff} TM0	n_{eff} TM1
532(1)	2.40	2.26	2.14	2.00
532(2)	2.40	2.26	2.13	1.99
532(3)	2.40	2.26	2.14	-
633(1)	2.32	-	2.08	-
633(2)	2.32	2.14	2.08	-
633(3)	-	-	-	-
1550(1)	2.04	-	1.88	-
1550(2)	2.04	-	1.88	-
1550(3)	2.04	-	1.88	-

Measurements of three different spots position for amorphous TiO_2 film have similar results in same wavelengths and different spots location. Spot location number three measurement with 532 nm wavelength is missing TM1 mode and spot position number one measurement with 633 nm wavelength has not found TE1 mode with higher effective index, n_{eff} = 2.14 compared to spot position number two in Tables 5 & 7. Also, there has been no mode found at 633 nm wavelength at spot position three. The reason comes from that the film quality at spot position three is not proper for measurement (edge of the film). Table 7 has approved the sample uniformity. Effective indices were found similar for all spots, however prism coupler could not find all modes at 532 nm and 632 nm wavelengths.

Variation of refractive index as a function of wavelength (513 nm-1551 nm) shown in Fig. 15. The plot is Cauchy dispersion model.

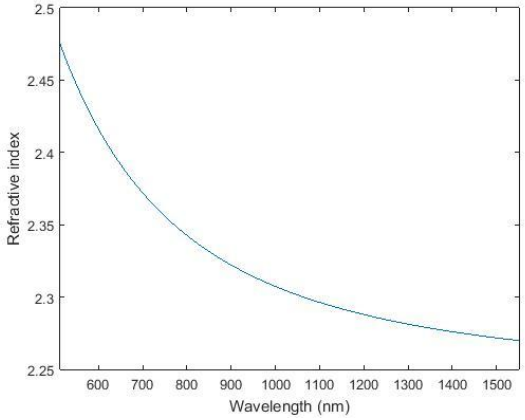

Figure 15. Cauchy dispersion fit for 500 nm amorphous TiO_2.

4.1.3 Nano Crystalline TiO_2

In this work, the thickness of nano laminates is found less than bulk TiO_2. Also, the thickness of nano laminates varied among the samples and can be explained by the process to process variation of ALD deposition (chapter 3). Additionally, the nucleation of TiO_2 may cause thickness variation as the different nucleation phases may have different growth rate. [18]

The substrate (corning glass 0211) refractive index has been measured by four wavelengths. The measurement result gives n=1.527 at 532 nm wavelength, n=1.523 at 633 nm wavelength, n=1.512 at 1064 nm wavelength and n=1.509 at 1550 nm wavelength.

Fig.16 is the intensity-angle plot of film S2 at 532 nm wavelength. There is found one TE propagation mode at n_{eff}=2.23 with higher index prism measurement.

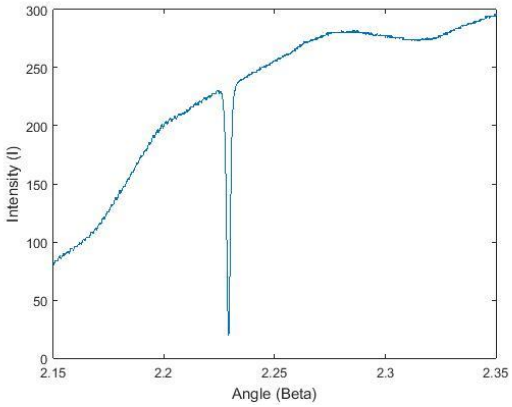

Figure 16. Intensity-angle plot of 532 nm laser in 183 nm thick S2 sample.

Fig.17 is an intensity-angle plot of sample S1 with 1550 nm laser. The plot is comparison of TE and TM propagation mode. There are found one TE mode with n_{eff}=1.65 and one TM mode with n_{eff}=1.50.

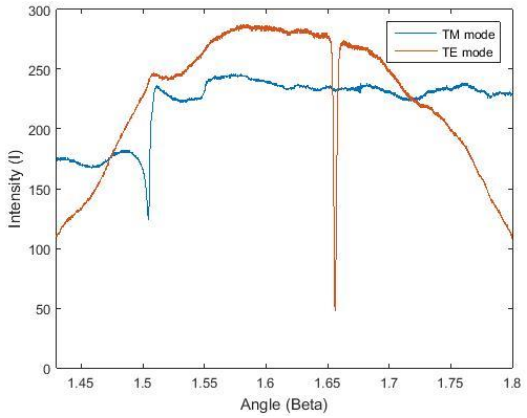

Figure 17. Comparison of sample 195 nm thick S1 film measurement at 1550 nm wavelength for TE and TM modes.

Fig.18 shows the S3 sample measurement with 1550 nm laser which yields one TE mode with n_{eff}= 1.68 and refractive index of n=2.32.

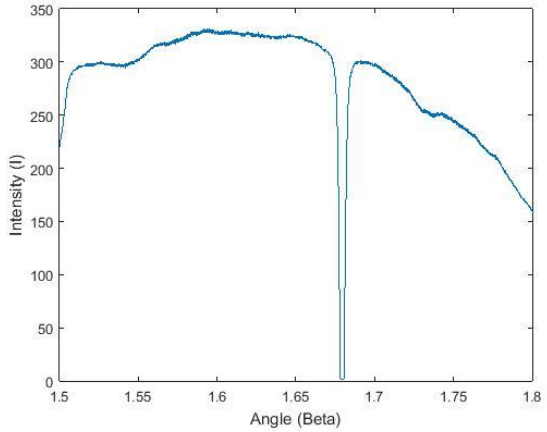

Figure 18. Intensity-angle plot of 173 nm S3 sample measurement at 1550 nm wavelength.

The measurement results are given in Tables 8 & 9. During measurement, no modes were found for film S0 at 532 nm and 1064 nm wavelengths. The reason is that the sample S0 has high surface roughness which makes high loss in waveguide. [18] Therefore, the film quality affects the film-thickness measurement is finding TE/TM modes.

Table 8. Experimental result for Nano Crystalline TiO_2 at 532 nm and 633 nm wavelengths.

Film ID	n_{eff}/ TE0 532 nm	n_{eff}/ TE1 532 nm	n (TE) 532nm	n_{eff}/ TM0 532 nm	n (TM) 532 nm	n_{eff}/ TE0 633 nm	n (TE) 633nm	n_{eff}/ TM0 633nm	n (TM) 633 nm
S0	-	-	-	2.02	2.32	2.11	2.34	1.99	2.37
S1	2.17	1.60	2.36	1.90	2.20	2.07	2.31	1.86	2.25
S2	2.23	1.58	2.45	1.96	2.31	2.11	2.37	1.86	2.30
S3	2.28	1.59	2.51	2.01	2.39	2.16	2.44	1.91	2.41
S4	2.29	1.58	2.52	2.03	2.43	2.13	2.42	1.88	2.40

The sample thicknesses are calculated at 532 nm wavelength for TE mode and the thicknesses have been found to be 197 nm, 178 nm, 171 nm and 168 nm for sample S1, S2, S3 and S4 respectively. The thickness has been calculated in close agreement (only 2, 3 nm difference) with simulation result.

Table 8 shows that the refractive indices are increasing when the thickness is decreasing from sample S0-S4 for fundamental modes at 532 nm wavelength. Effective indices of fundamental mode (TE0) are increasing as well as from S0-S4 samples at 532 nm wavelength but the n_{eff} of TE1 will be remained almost same (n_{eff} = 1.58-1.60) for all samples at same wavelength. In TM polarization, the fundamental propagation mode and refractive indices are increasing from samples S1-S4 at 532 nm wavelength. For TM polarization at 532 nm wavelength, there is a difference in effective indices around 0.26-0.29 for two polarizations in fundamental modes for samples S1-S4. At 633 nm wavelength, effective indices for fundamental modes for both polarization are changing randomly but refractive indices are increasing from samples S1-S4. There is a difference in fundamental polarizations (TE0 and TM0) in effective indices about 0.12 to 0.25 for samples S0-S4 at 633 nm wavelength.

Table 9 shows the results experiment for all nano crystalline samples at 1064 nm and 1550 nm wavelengths.

Table 9. Experimental results for nano crystalline TiO_2 at 1064 nm & 1551 nm wavelengths.

Film ID	n_{eff}/ TE0 1064nm	n (TE) 1064	n_{eff}/ TM0 1064nm	n (TM) 1064nm	n_{eff}/ TE0 1550nm	n (TE) 1550nm	n_{eff}/ TM0 1550nm	n (TM) 1550nm
S0	-	-	1.60	2.29	1.69	2.23	1.51	2.26
S1	-	-	1.56	2.20	1.65	2.22	1.50	2.37
S2	1.83	2.29	1.55	2.23	1.66	2.26	1.50	2.46
S3	-	-	1.55	2.30	1.68	2.32	1.50	2.58
S4	-	-	1.55	2.34	1.68	2.34	1.50	2.63

Thickness-index measurement of sample S2 has been detected one TE mode at 1064 nm wavelength and there have been detected three TM modes for all samples at same wavelength. Effective indices for TM modes are decreasing from samples S0-S4 but refractive indices are increasing for same samples at 1064 nm wavelength. Effective indices for fundamental TE mode are increasing at 1550 nm wavelength however refractive indices are increasing for samples S1-S4 at same wavelength in both polarizations.

The results in Table 9 shows that the both TE and TM modes have been detected at 1550 nm wavelength for samples S2, S3 and S4 in experiment but the simulation (Table 3) did not find the same modes. The reason could be that in simulation the refractive indices are presumed same $n = 2.30$ for both 633 nm and 1550 nm wavelengths but in measurement, each film-index measurement calculates refractive index for each wavelength and film thickness is calculated based on the propagation modes are found in experiment.

The results of wavelength dependence of n is estimated by Cauchy dispersion model in Fig. 18 for films S1-S4. In Fig.19, film S1 measurement is indicated by green curve, film S2 measurement is indicated by red curve, film S3 measurement is indicated by yellow curve and film S4 measurement is indicated by purple curve respectively. It has seen a bend in curve between 600 nm – 700 nm wavelength. It can be concluded that the absorption occurred between 532 nm- 1064 nm laser measurement however this Cauchy dispersion model does not generally work if there are absorption peaks present.

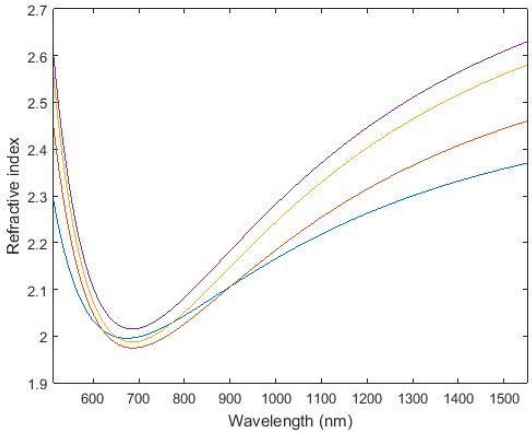

Figure 19. Cauchy dispersion fits for four films, S1-S4 measurements, green curve shows sample S0 fit, red curve shows sample S1 fit, yellow curve shows sample S3 fit and purple curve shows sample S4 fit.

4.1.4 Al_2O_3

The next sample study is Al_2O_3 film with Soda lime glass as a substrate. The similar measurements are done with four wavelengths as mentioned in previous measurements. There are found three modes for TE & TM polarizations at 532 nm wavelength. There are found two modes at 633 nm wavelength and one mode is found at 1064 nm and 1550 nm wavelengths. The wavelength dependence of *n* is estimated by Cauchy dispersion fit in Fig. 20.

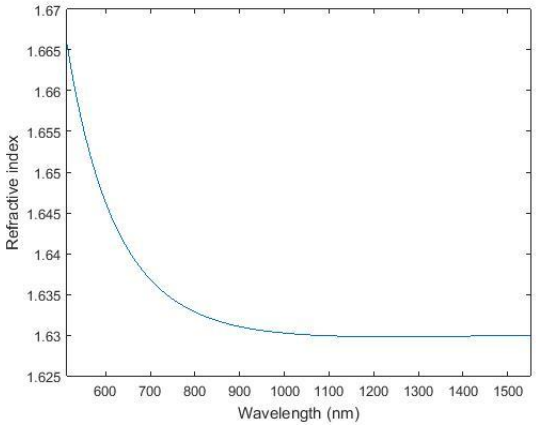

Figure 20. Cauchy dispersion fits for 970 nm Al_2O_3.

There are three modes found at 532 nm wavelength for each TE and TM polarization. Fig.21 shows the intensity plot as a function of β. There are three TM modes found with n_{eff}= 1.64, n_{eff} = 1.59 and n_{eff} = 1.51 with refractive index of n= 1.66.

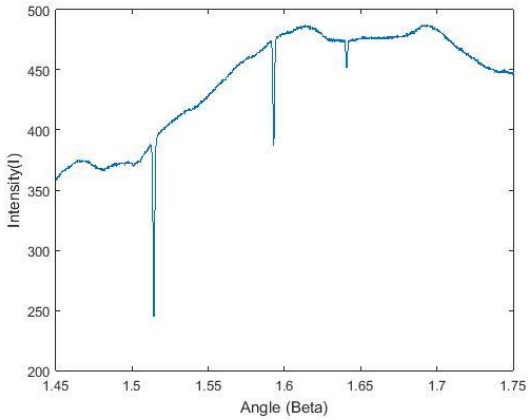

Figure 21. Intensity-angle plot of 970 nm Al_2O_3 film at 532 nm wavelength.

The result of measurement is presented in Table 10 and is shown that the refractive index is getting less when the wavelength is getting larger. The film thickness was measured about 0.92 µm with ellipsometery although prism coupling measurement has measured film thickness between 0.93 µm -1.02 µm. The thickness difference between two polarizations and wavelengths is not large and the difference reaches maximum to 0.09 µm.

Table 10. Experimental results of Al_2O_3 film for four wavelengths.

λ(nm)	n_{eff} TE0	n_{eff} TE1	n_{eff} TE2	n(TE)	Thick µm	n_{eff} TM0	n_{eff} TM1	n_{eff} TM2	n (TM)	Thick µm
532	1.64	1.59	1.51	1.66	0.97	1.64	1.59	1.51	1.66	1.02
633	1.63	1.56	-	1.65	0.93	1.55	1.61	-	1.63	1.01
1064	1.59	-	-	1.63	-	1.57	-	-	1.63	-
1550	1.55	-	-	1.63	-	1.55	-	-	1.66	-

A new simulation is done to find the exact thickness of the film which it is varied for the relevant n and neff of each polarization and wavelength to find the exact thickness is fitted for each wavelength. The simulation result found 0.97 µm film thickness which is approved the result of Table 10. There is found one mode (TE2) with n_{eff} = 1.46 at 633 nm wavelength and n_{eff} = 1.45 at 1064 nm wavelength in simulation which their effective indices are very close to the substrate index and they are too weekly guided so they were not observed in experiment.

4.1.5 Erbium Doped Al_2O_3

The last film has been measured with prism coupling is Er_2O_3-Al_2O_3. There are two modes observed during measurement for both polarizations (TE and TM modes) at 532 nm and 633 nm wavelengths, also one mode is observed for both polarizations at 1064 nm and 1550 nm wavelengths. The intensity curve is plotted in Fig. 22 for Er_2O_3-Al_2O_3 at 1550 nm wavelength with the effective index of n_{eff}=1.52 and refractive index of n=1.62.

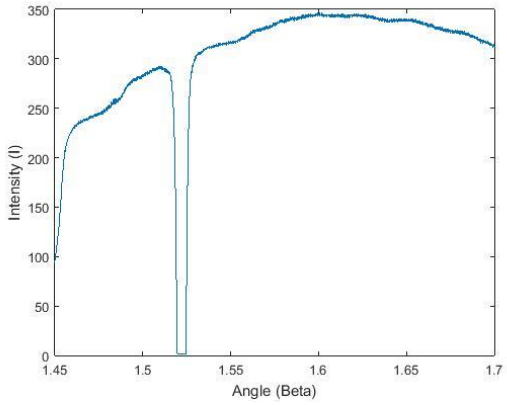

Figure 22. Intensity plot as a function of angle for 850 nm Er_2O_3-Al_2O_3 at 1550 nm wavelength.

The refractive index was constant in simulation for all wavelengths but in measurement it is calculated for TE and TM propagation modes for each wavelength. Metricon method calculates refractive index and thickness with using two equations which each equation includes one effective index. Therefore, it is needed at least two modes to solve the two equations with two known values (effective indices) and two unknown values (refractive

index and thickness). Wavelength dependence on refractive index curve is plotted by Cauchy dispersion model in Fig. 23. It is observed from Fig. 23 that the absorption affects the effective index at visible wavelengths. [33, 34] The results of measurement are presented in Table 11 at 532 nm, 633 nm, 1064 nm and 1550 nm wavelengths.

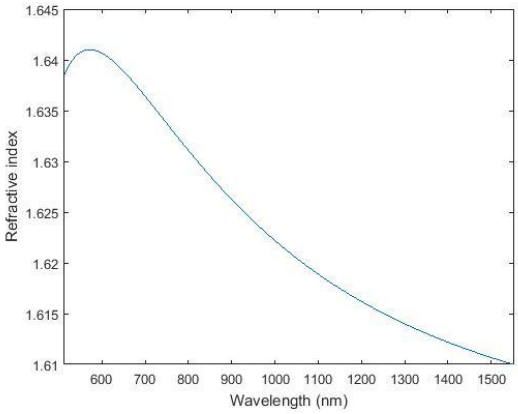

Figure 23. Cauchy dispersion fits for 850 nm Er_2O_3-Al_2O_3 at 532 nm -1551 nm wavelengths range.

Table 11. Experimental results of Er_2O_3-Al_2O_3 for four wavelengths.

λ (nm)	n_{eff} TE0	n_{eff} TE1	n (TE)	Thick µm	n_{eff} TM0	n_{eff} TM1	n (TM)	Thick µm
532	1.62	1.55	1.64	0.781	1.62	1.55	1.64	0.839
633	1.61	1.52	1.64	0.786	1.61	1.52	1.64	0.85
1064	1.56	-	1.62	-	1.55	-	1.62	-
1550	1.52	-	1.62	-	1.52	-	1.61	-

Refractive indices are same for both polarizations at same wavelengths. The thickness was measured around 0.925 µm with ellipsometer but the prism coupler calculated the thickness between 0.78 µm – 0.85 µm for both polarizations. In the new simulation, film thickness is found about 0.85 µm which is fitted all n_{eff} and n for all wavelengths better than film thickness of 0.925 µm.

4.2 Loss Measurement

In loss measurement, the fiber is moving above the sample and it measures the decay of propagation light in slabs. The measurement result of high loss should be appeared as an exponential form with no visible streak of propagating light. [1] Loss measurement is done for all films which possess modes with sharp dips. The measured losses for different films are shown in Table 12.

Table 12. Result of measured losses for different films.

Film ID /Thickness (nm)	Loss at 532 nm dB/cm	Loss at 1550 nm dB/cm
Amorphous TiO_2 / 500 nm	6.4	Very high
Nano crystalline /183 nm	9.4	4.1
Nano crystalline / 173 nm	Very high	5.7
Er_2O_3-Al_2O_3 / 850 nm	5.6	12.4

The loss result measurement of 500 nm amorphous TiO_2 at 532 nm wavelength and 183 nm Nano Crystalline TiO_2 (S2) at 1550 nm wavelength are presented in Figs. 24 & 25 respectively. The other measurements are affected by high scattering which are resulted high loss with large bumps. The loss achieved about 6.4 dB/cm for 500 nm amorphous TiO_2 and 4.1 dB/cm for 183 nm Nano Crystalline TiO_2.

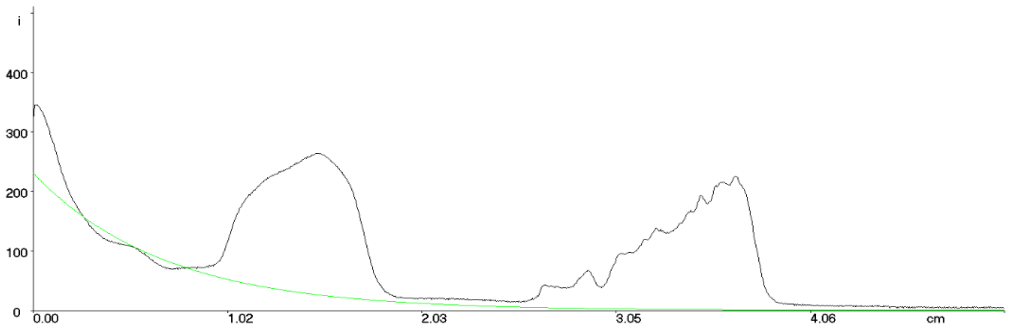

Figure 24. Loss measurement of 500 nm amorphous TiO_2 film at 532 nm wavelength. The loss value is 6.4 dB/cm at table location -2568 (2.40).

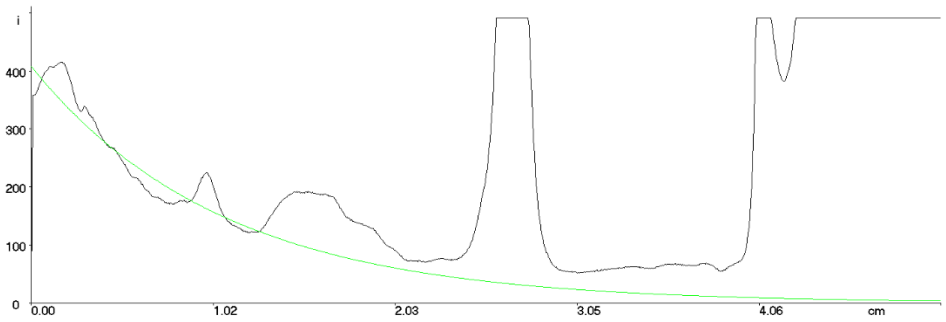

Figure 25. Loss measurement result of S2 film at 1550 nm wavelength. The loss values is 4.1 dB/cm at table position 469 (1.6659).

In the loss measurement, there are observed less bumps for TiO_2 at 532 nm and 183 nm S2 film at 1550 nm wavelengths. The highest bump is seen at measurement at 633 nm wavelength. Lower loss is achieved at smaller crystallites materials which they reach to 0.2 dB/mm. [2] In the films with high crystallite, scattering affect the light propagation and it causes larger bumps.

Chapter V
Conclusion

This work focused on the optical properties of the atomic layer deposited (ALD) thin films. Various thin films were fabricated for optical property characterization. One single-layer amorphous TiO_2 sample, five nanolaminates TiO_2 samples, one single-layer amorphous Al_2O_3 sample and one Er_2O_3- Al_2O_3 sample. In the nanolaminates TiO_2 thin films, thickness of TiO_2 was varied from 168 nm to 200 nm thick and it depends on the amount of total cycles. Amorphous TiO_2 deposited at pretty low temperature of 120 ^{0}C, nanolaminates TiO_2 thin films deposited at higher temperature of 250 ^{0}C, and Al_2O_3 and erbium doped are deposited at 300 ^{0}C. In this work, optical waveguides are optically characterized with refractive index and thickness by prism coupler device. The characterization setup of prism is equipped with four laser, which can be used for measurements at four different wavelengths, 532 nm, 633 nm, 1064 nm and 1550 nm. Using this setup is easy, accurate and fast to measure the thin films, which it is a good achievement. The optical quality of amorphous TiO_2 and Al_2O_3 proved that they were good enough to fabricate and use in waveguide applications.

From characterization results, refractive index of amorphous TiO_2 was found n = 2.46 in experiment and refractive index was calculated n = 2.44 in simulation at 532 nm wavelength for TE mode. Although, thickness was not calculated accurately in measurement (0.41 µm) at 532 nm wavelength, because one mode was missing with n_{eff} = 2.03 at the edge of the two prisms, but thickness with 0.5 µm fitted with all modes for both polarizations in simulation. All modes were found at 1064 nm and 1550 nm wavelengths in measurement, the thickness and the refractive indices were found same in both polarizations. The thickness is measured around 0.49 µm at 1064 nm wavelength which has very close result to ellipsometer (t = 0.5 µm) measurement. In nanolaminates

measurement result, refractive indices were increasing when the amount of TiO_2 laminates were increasing (S1-S4 films) but at the same time thicknesses were decreasing. This result approved the result in Table 2 at 633 nm wavelength, (refractive indices were found to decrease when the wavelength was switching to longer wavelength, however, at 1550 nm wavelength, refractive index was found same (n = 1.66) as at 532 nm wavelength). Thickness was calculated a bit thicker (0.970 µm) compared to ellipsometer measurement (0.918 µm). Refractive indices for Al_2O_3 are similar compared to Er_2O_3-Al_2O_3 result but the film thickness was calculated thinner (0.85 µm) compared to ellipsometer result measurement (0.925 µm). Al_2O_3 growth rate is getting low when it is mixed with Er_2O_3 so that could be the reason that the Er_2O_3-Al_2O_3 film thick was thinner compared to Al_2O_3 film. Loss measurement for different samples indicated that there was high propagation loss detected for the sample S3 at λ = 532 nm wavelength and sample TiO_2 at λ = 1550 nm wavelength. The losses are smaller for Er_2O_3-Al_2O_3 at λ = 532 nm wavelength which was approached to 0.56 dB/mm, same loss was resulted for sample S3 at λ = 1550 nm and for sample S2 at λ = 1550 nm, loss approached 0.4 dB/mm. It could be concluded that the scattering is affected all wavelengths however higher losses are occurred at shorter wavelength because the scattering is stronger in shorter wavelengths.

At the end, this work showed that ALD machine is a promising technique to fabricate thin films and to control the Er-ions in Er-doped and composition of nanolaminates. With prism coupling technique it is possible to measure films on transparent substrate and also it is possible to measure the films which are having close index with substrate index. However, there are still works needed in future to help the development of ALD process to achieve lower loss and higher growth rate.

References

[1] J.Aarik, A. Aidla, A. Kiisler, T. Uustare and V. Sammelselg, ‘‘*Effect of crystal structure on optical properties of TiO_2 films grown by atomic layer deposition*, ‘‘Thin Sol. Films, vol. 305, no. 1-2, pp. 270-273, 1997.

[2] Tapani Alasaarela,‘‘*Atomic layer deposited titanium dioxide in optical waveguiding applications,‘‘ Aalto University*,‘‘ School of Electrical engineering, June 2011.

[3] S.M. George, ‘‘*Atomic layer deposition: an overview,‘‘* Chemical reviews, vol.110, no. 1, 2010.

[4] John Rönn, *’’Fabrication and characterization of atomic-layer-deposited Er_2O_3 for optical amplifier devices*,’’ Aalto University, School of Electrical Engineering, December 2014.

[5] M. Ritala, K. Kukli, A. Rahtu, P.I. Räisänen, M. Leskelä, T. Sajavaara and J. Keinonen, *’’Atomic layer deposition of oxide thin films with metal alkoxides as oxygen sources,*’’ Science, vol. 288, no. 5464, 2000.

[6] T. Suntola, ’’*Atomic layer epitaxy*,’’ Materials Science Reports, vol. 4, no. 5, 1989.

[7] R. W. Johanson, A. Hultqvist and S. F. Bent, *’’A brief review of atomic layer deposition: from fundamentals to applications,*’’ Materials Today, vol. 17, no. 5, 2014.

[8] M. de Keijser and C. van Opdorp, *’’Atomic layer epitaxy of gallium arsenide with the use of atomic hydrogen,*’’ Applied Physics Letters, vol. 58, no. 11, 1991.

[9] H. B. Profijt, S. E. Potts, M.C. M. Van de Sanden and W. M. M. Kessels, *’’Plasma-assisted atomic layer deposition: basics, opportunities and challenges,*’’ Journal of vacuum science and technology A: vacuum, surfaces and films, vol. 29, no. 5, 2011.

[10] J. Wang, X. Deng, R. Varghese and A. Nikolov, *''Filling high aspect-ratio nano-structure by atomic layer depsotion and its applications in nano-optics devices and integrations,* '' J. Vac. Sci., vol. 23, no. 6, pp. 3209-3213, 2005.

[11] M. Ritala, M. Leskelä, L. Niinistö and T. Prohaska, *''Surface roughness reduction in atomic layer epitaxy growth of titanium dioxide thin film,*'' Thin Sol. Films, vol. 249, no. 22, pp. 155-1652, 1994.

[12] M. Di Ventra, S. Evoy and J. J. R. Helfin, ''*Introduction to nanoscale science and technology,*'' 1st ed. Kluwer Academic Publishers, 2004.

[13] A. Säynätjoki, L. Karvonen, T. Alasaarela, X. Tu, T. Y. Liow, M. Hiltunen, A. Tervonen, G. Q. Lo and S. Honkanen, *''Low-loss silicon slot waveguides and couplers fabricated with optical lithography and atomic layer deposition,*'' Optica Express, vol. 19, no. 27, 2011.

[14] K. Solehmainen, M. Kapulainen, P. Heimala and K. Polamo, *''Erbium doped waveguides fabricated with atomic layer deposition method,*'' IEEE Photon. Technol. Lett., vol. 16, no. 1, pp. 194-196, 2004.

[15] Picosun, ''PICOSUN™ R-series Atomic Layer Deposition (ALD) reactors.''[Online]. Available: http://www.picosun.com/en/products/picosun8482+r-series/

[16] The webpage of computational-photonics, http://computational-photonics.eu/, (valid October 2015).

[17]. T. Alasaarela, L. Karvonen, H. Jussila A. Säynätjoki, "*High-quality crystallinity controlled ALD TiO_2 for waveguiding applications*, Optics letters", Vol. 38, No. 20 (October 15,2013).

[18]. A. Tervonen, P. Pöyhönen, S. Honkanen, M. Tahkokorpi and S. Tammela, "*Examination of two-step fabrication methods for single-mode fiber compatible ion-exchanged glass waveguides"*, Applied Optics, Vol. 30, No.3, (20 January 1991).

[19] M.D. Groner, F.H. Faabreguette, J.W. Elam and S.M. George, '' *Low-Temperature Al_2O_3 Atomic Layer Deposition*'', Department of chemistry and Biochemistry and Department of Chemical Engineering, University of Colorado, December 2003.

[20] Webpage of Refractiveindex.info, (valid October 2015),

http://refractiveindex.info/?shelf=main&book=Al2O3&page=Malitson-o

[21] M. Born and E.Wolf, ‘’*Principles of Optics: Electromagnetic Theory of Propagation, Interference and Diffraction of light,’’ 6th ed.* Cambridge University Press, 1997.

[22] Lasse Karvonen, ‘*’Characterization Setup for Lithium Niobate waveguides’’*, Aalto University, Faculty of electronics, Communication and Automation, Master thesis, (First of January 2010).

[23] Young, H., *University Physics*, 8. Edition, USA, Addison-Wesley Publishing Company, 1992.

[24] Snyder, A. and Love J., *Optical waveguide Theory*, New York, Chapman and Hall, 1983.

[25] Yariv, A., and Yeh, P., *Photonics, 6. edition*, New York, Oxford University Press, 2007.

[26] Pollock, C., *Fundamentals of Optoelectronics*, 1. edition, New Delhi, CBLS, 2003.

[27] Butkov, E., *Mathematical Physics*, 1. edition, Reading, Addison-Wesley Publishing, 1968.

[28] Jackson, J.D., *Classical Electrodynamics*, 2. edition, New York, John Wiley and Sons, 1975.

[29] The wepage of Metricon, metricon.com/model-2000-m-overview/, (valid November 2015).

[30] D. Riihelä, M. Ritala, R. Matero and M. Lesklä, *’’Introducing atomic layer epitaxy for the deposition of optical thin films,*’’ Thin Sol. Films, vol. 289, no. 1-2, pp. 250-255, 1996.

[31] B.E.A Saleh and M.C. Tich, ‘*’Fundamental of photonics*,’’ 2nd ed. Wiley interscience, 2007.

[32] R. Puurunen, ‘*’Surface chemistry of atomic layer deposition: A case study for the trimethylaluminum/water process,*’’ J. Appl. Phys, vol. 97, p.121301, 2005.

[33] X. Multone, Y. Luo and P. Hoffmann, ‘*’Er-doped Sl2O3 thin films deposited by high-vacuum chemical vapor deposition (HV-CVD),*’’ Materials Science and Engineering: B, vol. 146, no. 1-3, 2008.

[34] M. Mahnke, S. Wiechman, H. J. Heider, O. Blume and J. Muller, ‘*’Aluminum Oxide Doped with Erbium, Titanium and Chromium for Active Integrated Optical Applications,’’* International Journal of Electronics and Communications, vol. 55, no. 5, 2001.

[35] R. Serna, J. M. Ballesteros, M. de Castro, J. Solis and C. N. Afonso, *’’Optically active Er-Yb doped glass films prepared by pulsed laser deposition,*’’ Journal of Applied Physics, vol. 84, no. 4, 1998.

[36] V. R. Almeidia, Q. Xu, C. A. Barrios and M. Lipson, ‘*’Guiding and confining light in void nanostructure,’’* Opt. Lett., vol. 29, no. 11, pp. 1209-1211, 2004.

[37] J. Leuthold, C. Koos and W. Freude, ‘*’Nonlinear silicon photonics,*’’ Nature Photons., vol. 4, no. 8, pp. 535-544, 2010.

[38] K. D. Vos, I. Bartolozzi, E. Schacht, P. Bienstman and R. Baets, *’’Silicon-on-insulator microring resonator for sensitive and label-free biosensing*,’’ Opt. Express, vol. 15, no. 12, pp. 7610-7615, 2007.

[39] P. K. Tien, ‘*’Light waves in thin films and integrated optics,’’* Appl. Opt., vol. 10, no. 11, pp. 2395-2413, 2011.

[40] R. Ulrich and R. Torge, ‘*’Measurement of thin film parameters with a prism coupler*,’’ Appl. Opt., vol. 12, no. 12, pp. 2901-2908, 1973.

[41] The webpage of J.A. woolam Co., www.jawoollam.com/tutorila_7.html, (valid December 2015).